Title

Dual-Site Cascade Oxygen Reduction Mechanism on SnO x /Pt–Cu–Ni for Promoting Reaction Kinetics

Journal

Journal of the American Chemical Society, 141(24)

ISSN

0002-7863

Authors

Shen, Xiaochen
Nagai, Tomoyuki
Yang, Feipeng
et al.

Publication Date

2019-06-19

DOI

10.1021/jacs.9b02286

Peer reviewed

Dual-Site Cascade Oxygen Reduction Mechanism on SnO_x/Pt−Cu−Ni for Promoting Reaction Kinetics

Xiaochen Shen,[†] Tomoyuki Nagai,[‡] Feipeng Yang,[†,§] Li Qin Zhou,[‡] Yanbo Pan,[†] Libo Yao,[†] Dezhen Wu,[†] Yi-Sheng Liu,[§] Jun Feng,[§] Jinghua Guo,[§] Hongfei Jia,[*,‡] and Zhenmeng Peng[*,†]

[†]Department of Chemical and Biomolecular Engineering, The University of Akron, Akron, Ohio 44325, United States
[‡]Material Research Department, Toyota Research Institute of North America, Ann Arbor, Michigan 48105, United States
[§]Advanced Light Source, Lawrence Berkeley National Laboratory, Berkeley, California 94720, United States

ABSTRACT: Designing highly active oxygen reduction reaction (ORR) catalysts is crucial to boost the fuel cell economy. Previous research has mainly focused on Pt-based alloy catalysts in which surface Pt is the solely active site and the activity improvement was challenged by the discovered scaling relationship. Herein we report a new concept of utilizing dual active sites for the ORR and demonstrate its effectiveness by synthesizing a SnO_x/Pt−Cu−Ni heterojunctioned catalyst. A maximum of 40% enhancement in the apparent specific activity, which corresponds to 10-fold enhancement on interface sites, is measured compared with pure Pt−Cu−Ni. Detailed investigations suggest an altered dual-site cascade mechanism wherein the first two steps occur on SnO_x sites and the remaining steps occur on adjacent Pt sites, allowing a significant decrease in the energy barrier. This study with the suggested dual-site cascade mechanism shows the potential to overcome the ORR energy barrier bottleneck to develop highly active catalysts.

Massive research efforts have been made to develop active and durable oxygen reduction reaction (ORR) catalysts, which is recognized as a key issue in polymer electrolyte membrane fuel cell (PEMFC) technology.[1−5] Pt-based alloy nanoparticles can exhibit significantly improved activity compared with pure Pt and are considered as one of the most important groups of ORR catalysts.[6−8] Mechanistic studies discovered that the activity improvement can be attributed to alloy-composition-induced modification of the electronic and geometric structure of surface Pt atoms, which serve as the active sites.[9,10] A large variety of Pt alloy nanoparticle catalysts have been prepared and investigated in the past decades, aiming at achieving higher ORR activity.[11,12] However, it appeared challenging to achieve further breakthroughs in the activity improvement since the $Pt_3Ni(111)$ study which was reported over 10 years ago.[11] This research difficulty could be explained using the recently discovered scaling relationship, which suggests that lowering the energy barrier of a certain step in the reaction pathway on an active site would result in increasing the barrier of other steps on the same site.[10,13,14] This implies the existence of a minimum energy barrier that can be achieved in sole-site catalysis and provides a plausible explanation for catalyst research in many reactions, for instance, selective methane oxidation,[15] ammonia synthesis,[16] and dehydrogenation.[17] Specific to the ORR research, this scaling relationship would set a limit in the activity improvement using Pt alloy catalysts.

In this work, we report the utilization of dual active sites by synthesizing a SnO_x/Pt−Cu−Ni heterojunctioned nanostructure to break the scaling relationship in ORR and promote the catalytic activity. Experimental and theoretical studies confirm a significant activity enhancement compared with pristine Pt−Cu−Ni and reveal a dual-site cascade mechanism wherein the first two steps occur on SnO_x sites, followed by transfer of the intermediate to adjacent Pt sites for the subsequent steps, leading to as high as 10-fold activity enhancement on these sites. This dual-site cascade mechanism breaks the scaling relationship that restricts Pt alloy catalysts and offers a plausible new approach to achieve high ORR activity on Pt alloys by introducing a second active site, which has not been well-studied previously.

Pt−Cu−Ni alloy nanoparticles on a carbon support were synthesized following a solid-state chemistry method involving electrochemical treatment to generate a clean Pt surface prior to use in this study.[3] Figure S1 shows a transmission electron microscopy (TEM) image of the Pt−Cu−Ni alloy nanoparticles after electrochemical treatment, which are uniformly distributed on the support with an average diameter of 6.1 nm. The high-resolution TEM (HRTEM) image (Figure S2) determines a lattice fringe spacing of 0.219 nm, which falls between those of the pure metal components, indicating the formation of an alloy structure.[4] The sample after SnO_x deposition, denoted as SnO_x/Pt−Cu−Ni, shows unchanged particle morphology and size (Figures 1A and S3). HRTEM characterizations exhibit a thin amorphous layer (guided with the yellow dotted line) that partially covers the particle, suggesting deposition of SnO_x on the Pt−Cu−Ni surface (Figures 1B and S4). This is further evidenced by energy-dispersive X-ray (EDX) analyses (Figure S5), the line scan profile (Figure S6), and elemental mapping (Figure 1C). Meanwhile, the measured lattice spacing of the inner alloy particle remains unchanged.

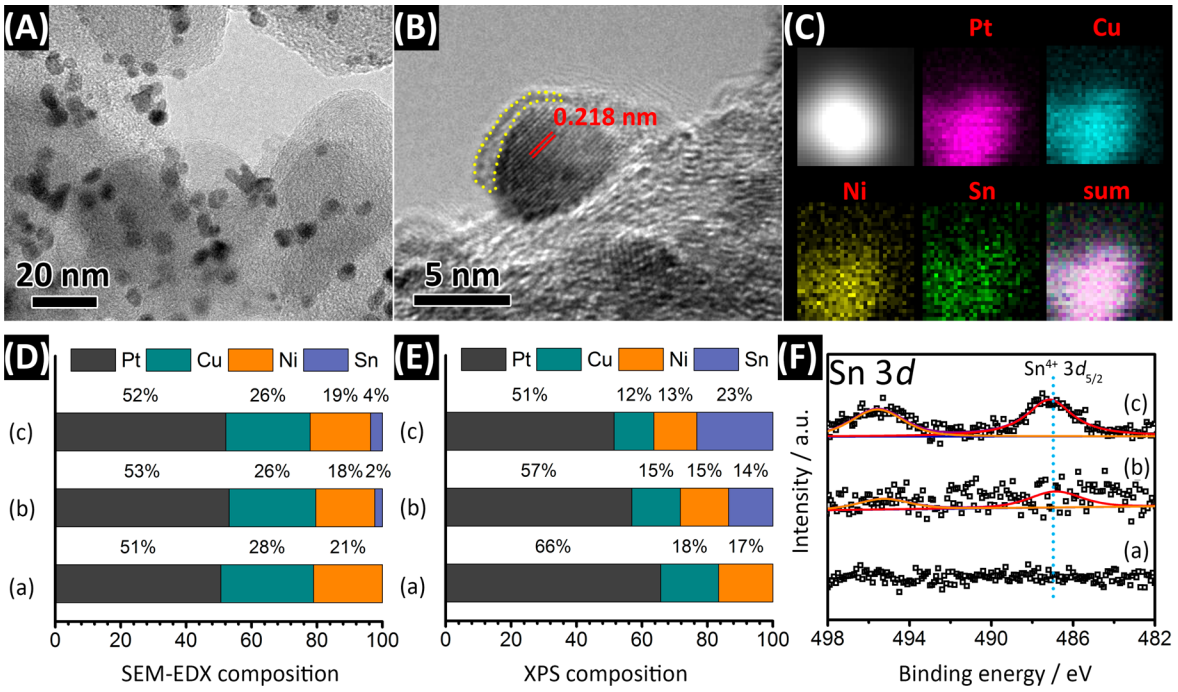

Figure 1. (A) TEM and (B) HRTEM images of SnO_x/Pt−Cu−Ni(60) nanoparticles. (C) STEM and elemental mapping of an individual SnO_x/Pt−Cu−Ni(60) nanoparticle. (D) SEM-EDX overall composition, (E) XPS surface composition, and (F) Sn 3d XPS spectra of (a) Pt−Cu−Ni nanoparticles prior to SnO_x deposition, (b) SnO_x/Pt−Cu−Ni(5), and (c) SnO_x/Pt−Cu−Ni(20) samples, respectively.

Both the obtained Pt−Cu−Ni and SnO_x/Pt−Cu−Ni samples were measured to determine their overall and surface compositions using quantitative EDX and X-ray photoelectron spectroscopy (XPS) analyses (Figure 1D,E and Table S1). The Pt−Cu−Ni nanoparticles prior to SnO_x deposition were determined to have an overall composition of $Pt_{51}Cu_{28}Ni_{21}$ and a surface composition of $Pt_{66}Cu_{18}Ni_{17}$, indicating a Pt-enriched surface as a result of dissolution of non-Pt surface atoms.[18−20] The Sn signals appear after SnO_x deposition, and the content grows with deposition time. The much higher surface Sn composition compared with the overall value is consistent with the TEM characterizations that SnO_x is deposited on the Pt−Cu−Ni particle surface. Both the overall and surface Pt:Cu:Ni ratios remain nearly constant before and after SnO_x deposition, suggesting little structural change, in agreement with the unchanged lattice spacing. Figures 1F and S7−S9 show high-resolution Sn 3d, Pt 4f, Cu 2p, and Ni 2p XPS spectra, respectively. The Sn 3d spectra show a distinct $3d_{3/2}$ peak at 495.6 eV and a $3d_{5/2}$ peak at around 487.1 eV, which is lower than the typically reported 487.4 eV for the Sn^{4+} $3d_{5/2}$ state in SnO_2.[21,22] This small decrease in the binding energy would correspond to a slightly reduced $Sn^{(4-\delta)+}$ state and/or amorphousness of the formed SnO_x layer.[23] We performed X-ray absorption near edge structure (XANES) characterizations (Figures S10−S12), which confirmed a primary Sn^{4+} oxidation state and the coherent amorphous structure. Nevertheless, all of these results confirm the successful deposition of SnO_x onto the Pt−Cu−Ni nanoparticle surface to generate heterojunctioned interfaces and show that the amount of SnO_x can be controlled by varying the deposition time (t_d).

The ORR catalytic properties of SnO_x/Pt−Cu−Ni were evaluated by electrochemical measurements in 0.1 M $HClO_4$. Figure 2A shows cyclic voltammetry (CV) curves of the SnO_x/Pt−Cu−Ni(t_d) (t_d = 0, 1, 2, 5, 10, 20, 40) samples. Noticeably, a pair of redox peaks between 0.6 and 0.8 V emerge along with the deposition of SnO_x and become more pronounced with a longer t_d, which are ascribable to the redox behavior associated with SnO_x.[24,25] The electrochemically active surface area (ECSA) of these catalysts is shown in Figure 2B. Prior to any SnO_x deposition, the Pt−Cu−Ni catalyst exhibits an ECSA value of 32.53 $m^2\ g_{Pt}^{-1}$. This value monotonically drops to 20.62 $m^2\ g_{Pt}^{-1}$ for the SnO_x/Pt−Cu−Ni(40) catalyst, which suggests that nearly 40% of the Pt−Cu−Ni is covered by SnO_x sites after 40 min of deposition.

The intrinsic ORR area-specific activity (SA) of these catalysts after *iR* compensation at 0.9 V vs RHE was determined from linear sweep voltammetry (LSV) measurements (Figure 2C) and is plotted as a function of t_d in Figure 2D. All of the electrochemical data are summarized in Table S2. It is noticeable that the prepared SnO_x/Pt−Cu−Ni(t_d) samples exhibited higher ORR activity than the Pt−Cu−Ni counterpart. The highest SA value was achieved using SnO_x/Pt−Cu−Ni(5) and was measured to be 1.60 mA cm_{Pt}^{-2}, which represents a nearly 40% activity enhancement compared with pristine Pt−Cu−Ni, outperforming the commercial Pt/C electrocatalyst (Figure S13). This provides unambiguous experimental evidence that reveals the promoting effect of SnO_x. This finding is consistent with previous studies of some other metal oxide/metal systems that observed improved activity but did not provide a detailed mechanistic discussion.[26−29] Interestingly, the SA exhibits a volcano trend with respect to t_d, which could be ascribed to structural change of SnO_x as a function of deposition time. TEM characterizations of the SnO_x/Pt−Cu−Ni(t_d) samples confirmed a continuous deposition process for SnO_x on Pt−Cu−Ni with elongation of t_d (Figures 1B and S14). Previous studies discovered significant size effects of the SnO_x catalyst, which were attributed to particle-size-induced structural transitions and chemical status variations in the SnO_x that alter the

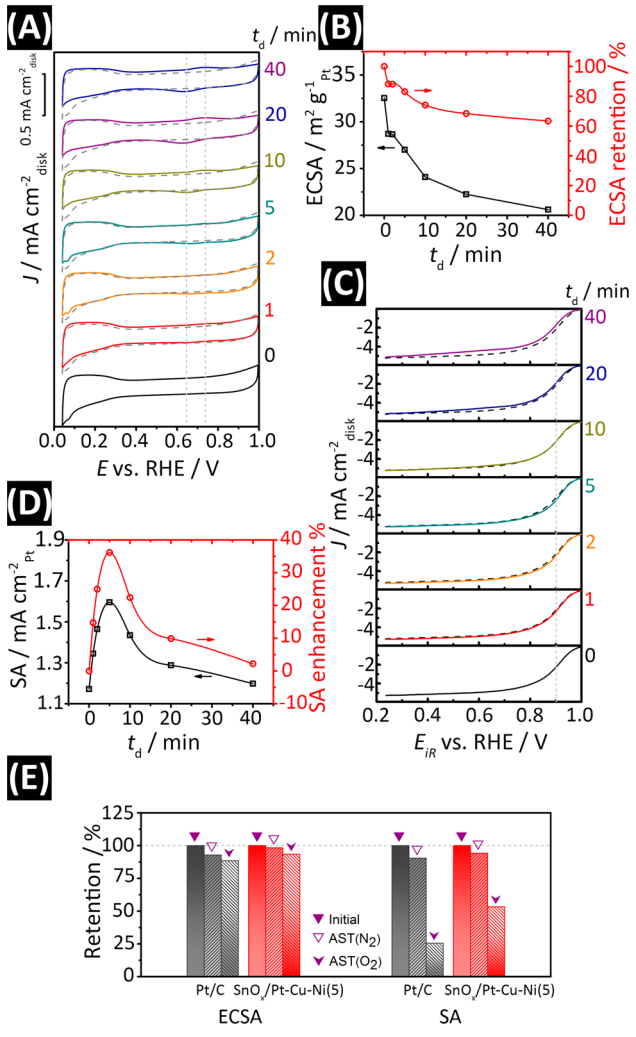

Figure 2. (A) CV curves, (B) ECSA data, (C) ORR LSV plots, and (D) SA and SA enhancement using SnO_x/Pt−Cu−Ni(t_d) (t_d = 0, 1, 2, 5, 10, 20, 40) catalysts (dashed plots indicate results for the t_d = 0 sample for reference). (E) ECSA and SA retention using SnO_x/Pt−Cu−Ni(5) catalyst before and after ASTs under N_2 and O_2 conditions.

catalytic properties.[30−32] It is likely that the SnO_x/Pt−Cu−Ni(5) catalyst possesses the most optimal SnO_x structure and thus exhibits the highest ORR activity.

Accelerated stability tests (ASTs) following both the DOE protocol (AST(N_2)) and a recent new protocol (AST(O_2)) were conducted to evaluate the long-term performance of the SnO_x/Pt−Cu−Ni(5) catalyst, as shown in Figure 2E.[33] The AST(N_2) results show only about 2% loss in the ECSA and a 6% drop in the SA value, indicating the outstanding stability of the catalytic structure. Even under the harsh AST(O_2) conditions, our sample still exhibits a significantly better durability (53% retention of SA) than commercial Pt/C (26% retention of SA). The TEM images and EDX results in Figures S15 and S16 confirm the well-retained morphology and structure of the alloy and only a partial loss of the SnO_x species, which can be ascribed to the electrochemical stability of the Pt−Cu−Ni alloy.[4,34]

To achieve insight into the mechanism behind the promoted ORR activity property of the SnO_x/Pt−Cu−Ni structure, we performed density functional theory (DFT) simulations of the reaction pathways (Figures S17−S19). Table S3 and Figure 3A

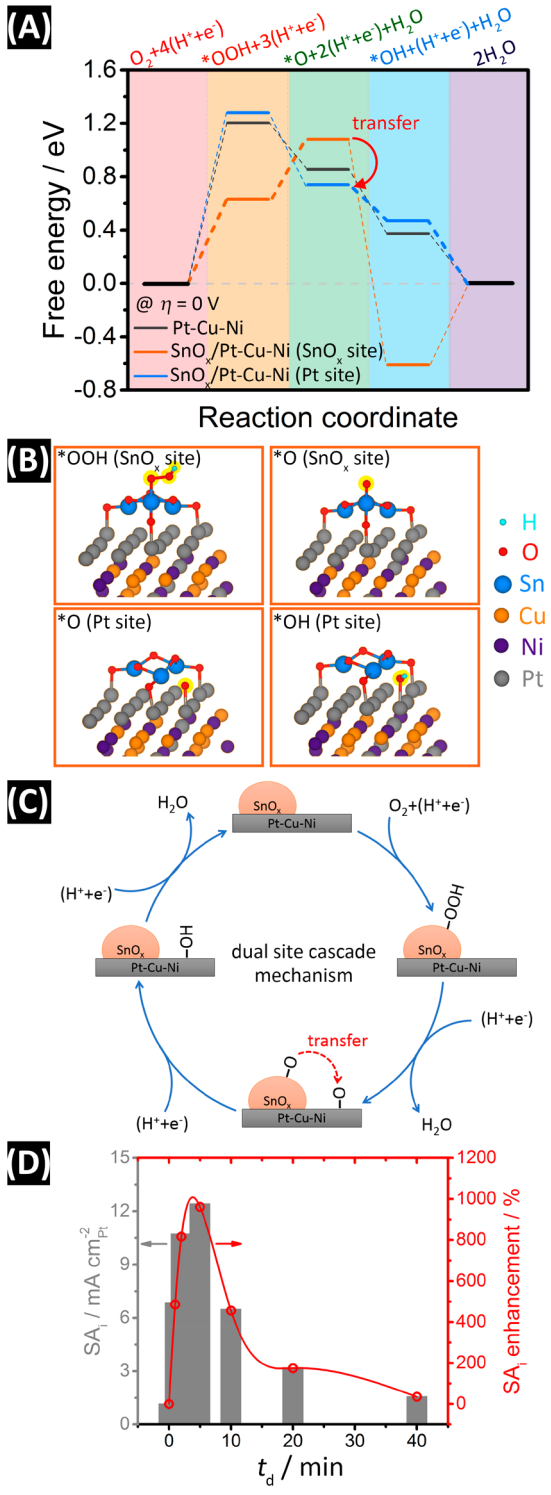

Figure 3. (A) ORR free energy diagrams for Pt−Cu−Ni and SnO_x/Pt−Cu−Ni. (B) DFT models of O, OH, and OOH adsorption on SnO_x/Pt−Cu−Ni. (C) Scheme of the dual-site cascade mechanism on SnO_x/Pt−Cu−Ni. (D) Estimated SA_i and SA_i enhancement using SnO_x/Pt−Cu−Ni(t_d) (t_d = 0, 1, 2, 5, 10, 20, 40) catalysts.

show the calculated energy data and diagrams for the possible ORR pathways that follow the associative mechanism, which involves generation of *OOH, *O, and *OH intermediates and has been largely agreed in previous studies.[10,13] On the pristine Pt−Cu−Ni, wherein surface Pt serves as the active site, the first reaction step appears to be rate-limiting. A significant

energy barrier of 1.20 eV is required to form the *OOH intermediate. Considering the SnO_x/Pt−Cu−Ni structure possesses two possible active sites (i.e., SnO_x site and Pt site), the ORR pathways on both sites were simulated. The pathway on the Pt site looks comparable to that on the pristine Pt−Cu−Ni, with only a slight change in the energy barrier (1.28 eV), which can be ascribed to a small electronic influence of SnO_x. This tiny influence, however, cannot account for the significantly promoted ORR kinetics.

On the other hand, the simulations of the SnO_x site show a different scenario. The energy barrier for the *OOH formation step is calculated to be 0.63 eV, which is significantly smaller than that on the Pt site. In the meantime, it exhibits energy barriers of 0.45 eV for the second step and 0.61 eV for the last *OH protonation step. Interestingly, the DFT data imply a dual-site pathway wherein SnO_x and Pt sites cooperate to be most kinetically favored. Specifically, O_2 is first protonated to generate *OOH and *O intermediates on SnO_x site because of the significantly lower energy barriers than on the Pt site. Then the *O intermediate on the SnO_x site would transfer to adjacent Pt site following a cascade adsorption mechanism to lower the system energy with a small energy barrier of 0.51 eV (Figure S20), on which it gets reduced further to *OH and eventually to H_2O in a barrierless downhill pathway. This plausible mechanism is supported by previous studies in which it was discovered that adsorbed chemical species would transfer between different sites.[35,36] More recently, activity promotion was discovered on transition metal (TM)−LiH composite materials in ammonia synthesis, which was attributed to the transfer of intermediates between the TM and LiH sites.[37]

A detailed scheme of this dual-site cascade ORR mechanism on SnO_x/Pt−Cu−Ni is illustrated in Figure 3B,C. This proposed new mechanism suggests that the promoted ORR kinetics is mostly attributed to adjacent SnO_x and Pt sites at interfaces of the two components. The intrinsic specific ORR activity of the Pt sites at SnO_x/Pt−Cu−Ni interfaces (SA_i) was estimated to evaluate the activity enhancement on these sites. The SA_i values are dramatically higher than the measured SA values, which are normalized using all available Pt sites (Figure 3D). The obtained SA_i of SnO_x/Pt−Cu−Ni(5) is estimated to be 12.43 mA cm_{Pt}^{-2}, which represents a nearly 10-fold enhancement compared to the pristine Pt−Cu−Ni and reveals dramatically promoted ORR kinetics following the dual-site cascade mechanism. Noticeably, the SA_i values also vary with SnO_x deposition time, which has been ascribed to the alteration in the deposited SnO_x size and consequently the SnO_x active site.

In summary, we have studied the ORR properties of SnO_x/Pt−Cu−Ni heterojunctioned structures synthesized by depositing SnO_x on the surface of Pt−Cu−Ni alloy nanoparticles. The obtained SnO_x/Pt−Cu−Ni catalysts exhibit significant enhancement in the ORR activity compared with pristine Pt−Cu−Ni. The measured specific activity shows a volcano dependence on the SnO_x deposition time, which is attributed to the altered SnO_x size that leads to different promoting effects. DFT simulations reveal a dual-site cascade reaction mechanism in which the first two ORR steps, which generate *OOH and *O intermediates, occur on SnO_x sites. The generated *O then transfer to adjacent Pt sites driven by cascade adsorption, allowing the following reaction steps to occur barrierlessly. This dual-site cascade reaction mechanism highlights the importance of adjacent SnO_x and Pt sites at SnO_x/Pt−Cu−Ni interfaces, with ORR on these sites being evaluated to exhibit as high as 10-fold enhancement in the activity. This work enlightens the design of dual-site catalysts to overcome the ORR energy barrier through a dual-site cascade reaction mechanism and opens a new era for fuel cell catalyst research.

AUTHOR INFORMATION

Corresponding Authors

*zpeng@uakron.edu

*hongfei.jia@toyota.com

ORCID

Feipeng Yang: 0000-0002-5470-3241

Jinghua Guo: 0000-0002-8576-2172

Zhenmeng Peng: 0000-0003-1230-6800

Notes

The authors declare no competing financial interest.

ACKNOWLEDGMENTS

The authors acknowledge Mr. Hisao Kato from Toyota Motor Corporation for technical discussions and advice. The HRTEM test was performed at the (cryo)TEM facility at the Liquid Crystal Institute at Kent State University, supported by the Ohio Research Scholars Program Research Cluster on Surfaces in Advanced Materials. The authors thank Dr. Min Gao for technical support with the TEM experiments. This research used resources of the Advanced Light Source, a DOE Office of Science User Facility Contract DE-AC02-05CH11231. The authors also thank Dr. Xuefei Feng for beamline support at ALS.

REFERENCES

(1) Kulkarni, A.; Siahrostami, S.; Patel, A.; Nørskov, J. K. Understanding catalytic activity trends in the oxygen reduction reaction. *Chem. Rev.* **2018**, *118* (5), 2302−2312.

(2) Li, M.; Zhao, Z.; Cheng, T.; Fortunelli, A.; Chen, C.-Y.; Yu, R.; Zhang, Q.; Gu, L.; Merinov, B.; Lin, Z.; Zhu, E.; Yu, T.; Jia, Q.; Guo, J.; Zhang, L.; Goddard, W. A.; Huang, Y.; Duan, X. Ultrafine jagged platinum nanowires enable ultrahigh mass activity for the oxygen reduction reaction. *Science* **2016**, *354* (6318), 1414−1419.

(3) Zhang, C.; Hwang, S. Y.; Trout, A.; Peng, Z. Solid-state chemistry-enabled scalable production of octahedral Pt−Ni alloy electrocatalyst for oxygen reduction reaction. *J. Am. Chem. Soc.* **2014**, *136* (22), 7805−7808.

(4) Zhang, C.; Sandorf, W.; Peng, Z. Octahedral Pt_2CuNi uniform alloy nanoparticle catalyst with high activity and promising stability for oxygen reduction reaction. *ACS Catal.* **2015**, *5* (4), 2296−2300.

(5) Zhang, C.; Shen, X.; Pan, Y.; Peng, Z. A review of Pt-based electrocatalysts for oxygen reduction reaction. *Front. Energy* **2017**, *11* (3), 268−285.

(6) Chong, L.; Wen, J.; Kubal, J.; Sen, F. G.; Zou, J.; Greeley, J.; Chan, M.; Barkholtz, H.; Ding, W.; Liu, D.-J. Ultralow-loading platinum-cobalt fuel cell catalysts derived from imidazolate frameworks. *Science* **2018**, *362* (6420), 1276−1281.

(7) Gocyla, M.; Kuehl, S.; Shviro, M.; Heyen, H.; Selve, S.; Dunin-Borkowski, R. E.; Heggen, M.; Strasser, P. Shape stability of octahedral PtNi nanocatalysts for electrochemical oxygen reduction reaction studied by in situ transmission electron microscopy. *ACS Nano* **2018**, *12* (6), 5306−5311.
(8) Guo, Y.-Z.; Yan, S.-Y.; Liu, C.-W.; Chou, T.-F.; Wang, J.-H.; Wang, K.-W. The enhanced oxygen reduction reaction performance on PtSn nanowires: The importance of segregation energy and morphological effects. *J. Mater. Chem. A* **2017**, *5* (27), 14355−14364.
(9) Escudero-Escribano, M.; Malacrida, P.; Hansen, M. H.; Vej-Hansen, U. G.; Velázquez-Palenzuela, A.; Tripkovic, V.; Schiøtz, J.; Rossmeisl, J.; Stephens, I. E. L.; Chorkendorff, I. Tuning the activity of Pt alloy electrocatalysts by means of the lanthanide contraction. *Science* **2016**, *352* (6281), 73−76.
(10) Seh, Z. W.; Kibsgaard, J.; Dickens, C. F.; Chorkendorff, I.; Nørskov, J. K.; Jaramillo, T. F. Combining theory and experiment in electrocatalysis: Insights into materials design. *Science* **2017**, *355* (6321), No. eaad4998.
(11) Stamenkovic, V. R.; Fowler, B.; Mun, B. S.; Wang, G.; Ross, P. N.; Lucas, C. A.; Marković, N. M. Improved oxygen reduction activity on $Pt_3Ni(111)$ via increased surface site availability. *Science* **2007**, *315* (5811), 493−497.
(12) Jia, Q.; Zhao, Z.; Cao, L.; Li, J.; Ghoshal, S.; Davies, V.; Stavitski, E.; Attenkofer, K.; Liu, Z.; Li, M.; Duan, X.; Mukerjee, S.; Mueller, T.; Huang, Y. Roles of Mo surface dopants in enhancing the ORR performance of octahedral PtNi nanoparticles. *Nano Lett.* **2018**, *18* (2), 798−804.
(13) Nørskov, J. K.; Rossmeisl, J.; Logadottir, A.; Lindqvist, L.; Kitchin, J. R.; Bligaard, T.; Jónsson, H. Origin of the overpotential for oxygen reduction at a fuel-cell cathode. *J. Phys. Chem. B* **2004**, *108* (46), 17886−17892.
(14) Anderson, A. B.; Roques, J.; Mukerjee, S.; Murthi, V. S.; Markovic, N. M.; Stamenkovic, V. Activation energies for oxygen reduction on platinum alloys: Theory and experiment. *J. Phys. Chem. B* **2005**, *109* (3), 1198−1203.
(15) Gani, T. Z. H.; Kulik, H. J. Understanding and breaking scaling relations in single-site catalysis: Methane to methanol conversion by Fe^{IV}═O. *ACS Catal.* **2018**, *8* (2), 975−986.
(16) Mehta, P.; Barboun, P.; Herrera, F. A.; Kim, J.; Rumbach, P.; Go, D. B.; Hicks, J. C.; Schneider, W. F. Overcoming ammonia synthesis scaling relations with plasma-enabled catalysis. *Nat. Catal.* **2018**, *1* (4), 269−275.
(17) Sun, G.; Zhao, Z.-J.; Mu, R.; Zha, S.; Li, L.; Chen, S.; Zang, K.; Luo, J.; Li, Z.; Purdy, S. C.; Kropf, A. J.; Miller, J. T.; Zeng, L.; Gong, J. Breaking the scaling relationship via thermally stable Pt/Cu single atom alloys for catalytic dehydrogenation. *Nat. Commun.* **2018**, *9* (1), 4454.
(18) Strasser, P.; Koh, S.; Anniyev, T.; Greeley, J.; More, K.; Yu, C.; Liu, Z.; Kaya, S.; Nordlund, D.; Ogasawara, H.; Toney, M. F.; Nilsson, A. Lattice-strain control of the activity in dealloyed core−shell fuel cell catalysts. *Nat. Chem.* **2010**, *2*, 454.
(19) Malacrida, P.; Sanchez Casalongue, H. G.; Masini, F.; Kaya, S.; Hernández-Fernández, P.; Deiana, D.; Ogasawara, H.; Stephens, I. E. L.; Nilsson, A.; Chorkendorff, I. Direct observation of the dealloying process of a platinum−yttrium nanoparticle fuel cell cathode and its oxygenated species during the oxygen reduction reaction. *Phys. Chem. Chem. Phys.* **2015**, *17* (42), 28121−28128.
(20) Srivastava, R.; Mani, P.; Hahn, N.; Strasser, P. Efficient oxygen reduction fuel cell electrocatalysis on voltammetrically dealloyed Pt−Cu−Co nanoparticles. *Angew. Chem., Int. Ed.* **2007**, *46* (47), 8988−8991.
(21) Liu, H.; Hu, R.; Sun, W.; Zeng, M.; Liu, J.; Yang, L.; Zhu, M. Sn@SnO_x/C nanocomposites prepared by oxygen plasma-assisted milling as cyclic durable anodes for lithium ion batteries. *J. Power Sources* **2013**, *242*, 114−121.
(22) Hou, X.; Hu, Y.; Jiang, H.; Li, Y.; Li, W.; Li, C. One-step synthesis of SnO_x nanocrystalline aggregates encapsulated by amorphous TiO_2 as an anode in Li-ion battery. *J. Mater. Chem. A* **2015**, *3* (18), 9982−9988.
(23) Li, Y.; Xin, Q.; Du, L.; Qu, Y.; Li, H.; Kong, X.; Wang, Q.; Song, A. Extremely sensitive dependence of SnO_x film properties on sputtering power. *Sci. Rep.* **2016**, *6*, 36183.
(24) Meenakshi, S.; Sridhar, P.; Pitchumani, S. Carbon supported Pt−Sn/SnO_2 anode catalyst for direct ethanol fuel cells. *RSC Adv.* **2014**, *4* (84), 44386−44393.
(25) Lim, D.-H.; Choi, D.-H.; Lee, W.-D.; Park, D.-R.; Lee, H.-I. The effect of Sn addition on a Pt/C electrocatalyst synthesized by borohydride reduction and hydrothermal treatment for a low-temperature fuel cell. *Electrochem. Solid-State Lett.* **2007**, *10* (5), B87−B90.
(26) Samjeské, G.; Nagamatsu, S.-i.; Takao, S.; Nagasawa, K.; Imaizumi, Y.; Sekizawa, O.; Yamamoto, T.; Uemura, Y.; Uruga, T.; Iwasawa, Y. Performance and characterization of a Pt−Sn(oxidized)/C cathode catalyst with a SnO_2-decorated Pt_3Sn nanostructure for oxygen reduction reaction in a polymer electrolyte fuel cell. *Phys. Chem. Chem. Phys.* **2013**, *15* (40), 17208−17218.
(27) Masuda, T.; Fukumitsu, H.; Fugane, K.; Togasaki, H.; Matsumura, D.; Tamura, K.; Nishihata, Y.; Yoshikawa, H.; Kobayashi, K.; Mori, T.; Uosaki, K. Role of cerium oxide in the enhancement of activity for the oxygen reduction reaction at Pt−CeO_x nanocomposite electrocatalyst - an in situ electrochemical X-ray absorption fine structure study. *J. Phys. Chem. C* **2012**, *116* (18), 10098−10102.
(28) Selvaganesh, S. V.; Selvarani, G.; Sridhar, P.; Pitchumani, S.; Shukla, A. K. A durable PEFC with carbon-supported Pt−TiO_2 cathode: A cause and effect Study. *J. Electrochem. Soc.* **2010**, *157* (7), B1000−B1007.
(29) Nagasawa, K.; Takao, S.; Nagamatsu, S.-i.; Samjeské, G.; Sekizawa, O.; Kaneko, T.; Higashi, K.; Yamamoto, T.; Uruga, T.; Iwasawa, Y. Surface-regulated nano-SnO_2/Pt_3Co/C cathode catalysts for polymer electrolyte fuel cells fabricated by a selective electrochemical Sn deposition method. *J. Am. Chem. Soc.* **2015**, *137* (40), 12856−12864.
(30) Jiang, L.; Sun, G.; Zhou, Z.; Sun, S.; Wang, Q.; Yan, S.; Li, H.; Tian, J.; Guo, J.; Zhou, B.; Xin, Q. Size-controllable synthesis of monodispersed SnO_2 nanoparticles and application in electrocatalysts. *J. Phys. Chem. B* **2005**, *109* (18), 8774−8778.
(31) Ahn, H.-J.; Choi, H.-C.; Park, K.-W.; Kim, S.-B.; Sung, Y.-E. Investigation of the structural and electrochemical properties of size-controlled SnO_2 nanoparticles. *J. Phys. Chem. B* **2004**, *108* (28), 9815−9820.
(32) Khan, N.; Athar, T.; Fouad, H.; Umar, A.; Ansari, Z. A.; Ansari, S. G. Application of pristine and doped SnO_2 nanoparticles as a matrix for agro-hazardous material (organophosphate) detection. *Sci. Rep.* **2017**, *7*, 42510.
(33) Huang, X.; Zhao, Z.; Cao, L.; Chen, Y.; Zhu, E.; Lin, Z.; Li, M.; Yan, A.; Zettl, A.; Wang, Y. M.; Duan, X.; Mueller, T.; Huang, Y. High-performance transition metal−doped Pt_3Ni octahedra for oxygen reduction reaction. *Science* **2015**, *348* (6240), 1230−1234.
(34) Mao, J.; Chen, W.; He, D.; Wan, J.; Pei, J.; Dong, J.; Wang, Y.; An, P.; Jin, Z.; Xing, W.; Tang, H.; Zhuang, Z.; Liang, X.; Huang, Y.; Zhou, G.; Wang, L.; Wang, D.; Li, Y. Design of ultrathin Pt-Mo-Ni nanowire catalysts for ethanol electrooxidation. *Sci. Adv.* **2017**, *3* (8), No. e1603068.
(35) Conner, W. C.; Falconer, J. L. Spillover in heterogeneous catalysis. *Chem. Rev.* **1995**, *95* (3), 759−788.
(36) Prins, R. Hydrogen spillover. facts and fiction. *Chem. Rev.* **2012**, *112* (5), 2714−2738.
(37) Wang, P.; Chang, F.; Gao, W.; Guo, J.; Wu, G.; He, T.; Chen, P. Breaking scaling relations to achieve low-temperature ammonia synthesis through LiH-mediated nitrogen transfer and hydrogenation. *Nat. Chem.* **2017**, *9*, 64.